ISSN 1063-7834, Physics of the Solid State, 2017, Vol. 59, No. 8, pp. 1600–1606. © Pleiades Publishing, Ltd., 2017.
Original Russian Text © G.S. Shakurov, R.I. Khaibullin, V.G. Tomas, D.A. Fursenko, R.I. Mashkovtsev, O.N. Lopatin, A.G. Nikolaev, B.P. Gorshunov, E.S. Zhukova, 2017, published in Fizika Tverdogo Tela, 2017, Vol. 59, No. 8, pp. 1576–1582.

IMPURITY CENTERS

Submillimeter ESR Spectra of Fe^{2+} Ions in Synthetic and Natural Beryl Crystals

G. S. Shakurov[a,*], R. I. Khaibullin[a], V. G. Tomas[b], D. A. Fursenko[b], R. I. Mashkovtsev[b], O. N. Lopatin[c], A. G. Nikolaev[c], B. P. Gorshunov[d, e], and E. S. Zhukova[d, e]

[a] *Kazan Physicotechnical Institute, Kazan Scientific Center, Russian Academy of Sciences, Kazan, Russia*
[b] *Institute of Geology and Mineralogy, Siberian Branch, Russian Academy of Sciences, Novosibirsk, Russia*
[c] *Kazan (Volga region) Federal University, Kazan, Russia*
[d] *Prokhorov General Physics Institute, Russian Academy of Sciences, Moscow, Russia*
[e] *Moscow Institute of Physics and Technology (State University), Dolgoprudnyi, Moscow region, 141700 Russia*
**e-mail: shakurov@kfti.knc.ru*

Received February 14, 2017

Abstract—Electron spin resonance spectra of non-Kramers bivalent iron (Fe^{2+}) ions have been detected in synthetic and natural beryl crystals with an iron impurity. The observed ESR spectra have been attributed to resonance transitions of Fe^{2+} ions from the ground (singlet) state to excited (doublet) levels with the splitting $\Delta = 12.7$ cm^{-1} between the levels. The experimental angular and frequency dependences of the resonance field of the ESR signal have been described by the spin Hamiltonian with the effective spin $S = 1$. The analysis of the ESR data and optical absorption spectra indicates that the Fe^{2+} ions are situated in tetrahedral positions and substitute Be^{2+} cations in the beryl structure.

DOI: 10.1134/S1063783417080236

1. INTRODUCTION

Electron spin resonance spectroscopy of Fe^{2+} ions in crystals is currently represented by a few works. Information available in literature does not allow predicting the possibility of the observation of Fe^{2+} ESR in various structures. The ESR signals for the positions of rhombic and a lower symmetry as a rule cannot be observed with the use of the standard X- and Q-band apparatus. This is associated with the fact the spin states of non-Kramers Fe^{2+} ions in these cases are singlets, the energy intervals between which are greater than the energy quanta of standard spectrometer. This situation takes place, e.g., in ammonium Tutton's salt crystals [1] and forsterite (Mg_2SiO_4) [2]. In the case of axial and cubic symmetry, the ground energy level of a Fe^{2+} ions is often singlet as well, and degenerate levels lie too far from it to observe the resonance between these levels. Such systems are exemplified by α-Al_2O_3 [3] and ZnS [4]. The ESR signal can be detected only if the ground state is degenerate in the magnetic field, as in, e.g., MgO crystal [5]. In this case, interpretation of the spectra on the basis of a single observed transition requires serious theoretical analysis.

Obviously, to extend the number of crystals in which the observation of the ESR spectra of Fe^{2+} ions is possible, higher resonance frequency and, accordingly, the magnetic field of the ESR spectrometers are required. Tunable sources of the subterahertz range can also be used in relatively weak magnetic fields. In these cases, resonance transitions from the ground state to the excited states of Fe^{2+} ions can be observed for both low-symmetry and high-symmetry crystals. However, the power of microwave sources decreases with an increase in frequency and, in addition, an additional absorption associated with the phonon spectrum of the crystal appears in the terahertz range, which also restricts the possibility of observing the ESR spectra. Thus, the ESR spectroscopy of Fe^{2+} ions in crystal is a challenging experimental problem.

In this work, we present the results of the experimental investigation of submillimeter ESR spectra of Fe^{2+} ions in a synthetic beryl ($Be_3Al_2Si_6O_{18}$) and natural colorless goshenite crystals. To compare the found results with the literature data we also measured the optical spectra of the crystals under investigation.

The beryl crystal has a hexagonal symmetry (space group $P6/mcc$) and trivalent aluminum cations in its structure are surrounded by oxygen anions forming octahedra, whereas bivalent beryllium and tetravalent silicon ions are surrounded by oxygen tetrahedra, respectively. The point symmetry of the Al, Be, and Si positions is D_3, D_2 and Cs, respectively. The first works [6, 7] devoted to the investigation of iron ions in beryl

by ESR were published more than half a century ago. By now, quite many works devoted primarily to Fe^{3+} ions and Fe^{3+}–Fe^{3+} exchange pairs have been published (see, e.g., [8]). There is only one communication on the observation of the ESR signals of Fe^{2+} ions in the structural position of beryllium [9].

The specificity of the crystal lattice of beryl is the presence of structural channels situated along the sixth-order axis. The beryl channels can be filled by individual water molecules during the growth under the conditions of hydrothermal synthesis and in natural samples; the fraction of water can be as high as 3% by weight. The individual water molecules in a high-symmetry crystal environment form a model system for studying the properties of water under confinement. We recently studied the properties of water in beryl by dielectric terahertz spectroscopy [10, 11]. It was shown, in particular, that the spatially structured arrangement of water in the beryl channels leads to virtual ferroelectricity [12]. A possible influence of water on the ESR spectra is also important, as discussed below. On the other hand, the paramagnetic ions and complexes can be embedded into the beryl channels [13, 14]. This is of great interest, since the ESR linewidths are very small in the case of localization of paramagnetic centers, which makes the crystal promising for quantum memory systems.

2. EXPERIMENTAL

Synthetic beryl crystals with an iron impurity were grown by the hydrothermal method [15] in laboratory autoclaves with a volume of about 200 mL by the synthesis from oxides: synthetic quartz SiO_2, melted electrocorund Al_2O_3 and a BeO compound of a chemical purity grade. The crystals were grown onto nucleation plates cut from synthetic beryls along the $\{5.5.\overline{10}.6\}$ direction. Multicomponent acidic fluoride solutions [16] were used as a mineralizer. To avoid the inclusion of components of the autoclave still into the beryl crystals, the beryl and mineralizer components and the nucleation plates were placed into a vacuum-tight welded golden bulb with a volume of about 100 mL [17], in which the growth actually occurred. The growth conditions of beryl crystals were as follows: a temperature of ~600°C and a pressure of ~1.5 kbar.

Chemical composition of beryl crystals

Oxide	Sample 1	Sample 2
SiO_2	66.32	66.52
BeO	13.52	13.33
Al_2O_3	18.48	18.2
Fe_2O_3	0.08	0.52
V_2O_3	0.37	0
Li_2O	0.30	0
Na_2O	0	0.05
K_2O	0	0.01
Cs_2O	0	0.03
L/a (H_2O)	1.32	0.88
Σ	100.39	99.54

L/a stand for losses during annealing.

We studied the samples of (no. 1) green and (no. 2) bluish color, whose color is caused by the main dopant of the 3*d* element (V^{3+} and $Fe^{2+,\,3+}$ for nos. 1 and 2, respectively). The chemical analysis of the composition of the beryls (see the table) was performed by the inductively coupled plasma–atomic emission spectroscopy (ICP–AES) for main components (with an accuracy of 1%) and inductively coupled plasma–mass spectroscopy (ICP–MS) for impurities (with an accuracy of 10%). The chemical formulas of the samples recalculated according to the results of the analysis under the assumption that all losses during annealing were caused by removing water from the beryl structure were as follows:

$$(Be_{2.938}Si_{0.002}Fe_{0.002}Li_{0.058})_{\Sigma=3}(Al_{1.979}Fe_{0.003}V_{0.027})_{\Sigma=2.01\approx2}Si_6O_{18}\{(H_2O)_{0.398}Li_{0.052}\}$$

(sample 1),

$$(Be_{2.912}Si_{0.051})_{\Sigma=2.96\approx3}(Al_{1.950}Fe_{0.036})_{\Sigma=1.99\approx2}Si_6O_{18}\{(H_2O)_{0.267}Na_{0.009}K_{0.001}Cs_{0.001}\}$$

(sample 2).

The ESR spectra of Fe^{2+} were observed only in crystal no. 2. To study the influence of water on the ESR spectra, this sample was annealed for 24 h in vacuum at a high temperature of 1000°C. The detection of the ESR spectra was repeated after annealing (dehydration) of the sample. This sample is further referred to as no. 4. The signals of bivalent iron were also detected for a natural colorless beryl sample—goshenite from the Middle Urals deposit (sample 3). The sample was characterized by a high transparency and a pale bluish tint. The percentage and valence state of iron in the natural sample were studied in our previous works [18, 19]. According to the elemental energy dispersive X-ray (EDX) spectroscopy microanalysis and the Mössbauerr spectroscopy data, the contamination of the iron impurity in the natural crystal was much lower than in its synthetic analog (sample 2), on the order of 0.15 at %. As was found, the major fraction (~80% of the total amount) of the iron impurity occurred in the form of bivalent iron ions localized in (60%) octahe-

dral or (20%) tetrahedral lattice sites isomorphicly substituting aluminum and beryllium, respectively (see the table in [19]).

The ESR spectra were measured on a wide-band ESR spectrometer using backward-wave oscillators as microwave sources. The detailed description of the design of the spectrometer can be found in [20]. All measurements were carried out at liquid-helium temperature.

The optical absorption spectra were detected on a Shimadzu UV-3600 spectrophotometer in the wavelength range of 185–3200 nm at room temperature.

3. RESULTS

3.1. ESR in a Submillimeter Range

The ESR spectra attributed to bivalent iron ions were observed in the frequency range of 350–401 GHz. In Fig. 1, they are shown for various frequencies at the orientation $\mathbf{B}_0 \parallel \mathbf{c}$ of the crystal, where $\mathbf{B}_0$ is the static magnetic field and c is the fundamental symmetry axis of the beryl crystal. In sample 2, the ESR line featured an unresolved structure composed of at least two lines. In sample 3, only a weak broad line was detected, whose position coincided with the position of the most intense line in sample 2. Based on the frequency–field dependence for sample 2 (Fig. 2), we concluded that the singlet–doublet resonance transitions with a zero-field splitting of ~12.7 cm^{-1} were observed and the levels of the doublet are in turn split by a small energy gap. Figure 2 shows only the intense line of the structure. We failed to measure the zero-field splitting by a direct method owing to a low power of the microwave oscillator in this range. In the frequency range higher that the zero-field splitting, sample 2 exhibited a weak line in the low-field part of the spectrum associated with the singlet–singlet resonance transition. This line was not studied owing to a low signal-to-noise ratio. It is marked by the arrow in Fig. 1. We succeeded to measure this line only at a few frequencies and the respective values are also shown on the frequency–field dependence in Fig. 2. The angular dependence of the singlet–doublet resonance transition of Fe^{2+} ions in beryl (Fig. 3) was measured in the $(10\bar{1}0)$ plane. The ESR signals were not detected in the (0001) plane. The angular dependence did not reveal magnetically nonequivalent centers, but the range of measured angles appeared to be incomplete. In this case, there were limitations associated with the presence of structural water in the beryl channels. As was found in our previous works [10, 11], water molecules intensively absorb submillimeter waves with the polarization $\mathbf{E}_1 \perp \mathbf{c}$ ($\mathbf{E}_1$ is the microwave electric field). The ESR spectra were observed under the condition $\mathbf{B}_1 \perp \mathbf{B}_0$ and the spectrometer utilized the Voigt geometry; i.e., $\mathbf{k} \perp \mathbf{B}_0$, where $\mathbf{k}$ is the wave vector of the plane wave incident to the sample.

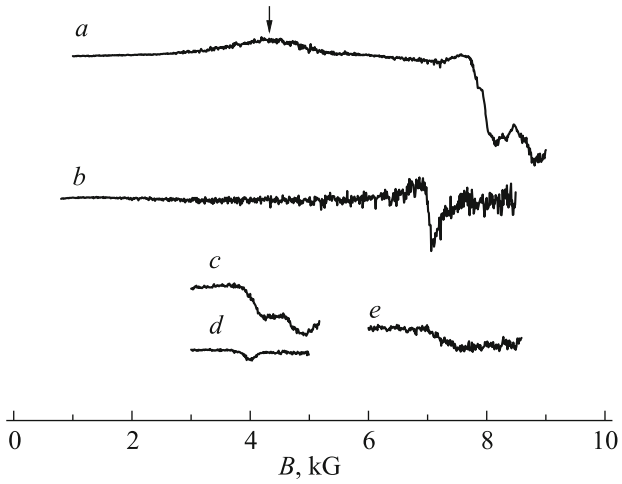

Fig. 1. Electron spin resonance spectra of Fe^{2+} ions in beryl crystals: samples (*a*, *c*) 2, (*b*, *d*) 4, and (*e*) 3. The arrow marks a weak broad line of the singlet–singlet transition in sample 2. The frequencies are (*a*) 401.5, (*b*, *e*) 399.5, (*c*) 391.2, and (*d*) 391 GHz. The orientation is $\mathbf{B}_0 \parallel \mathbf{c}$.

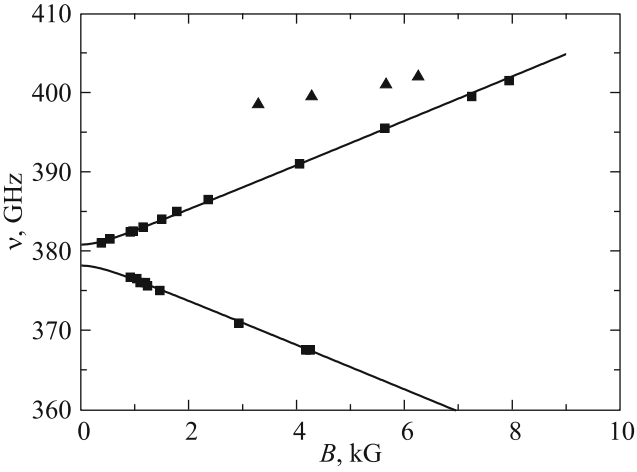

Fig. 2. Field dependence of the resonance transition frequencies of Fe^{2+} ions in beryl (sample 2). Squares are the experiment (the position of the most intense line of the structure are indicated); the line is the simulation. Triangles represent the singlet–singlet resonance transition.

Therefore, when the orientation deviated from $\mathbf{B}_0 \parallel \mathbf{c}$ ($\mathbf{E}_1 \parallel \mathbf{c}$) toward $\mathbf{B}_0 \perp \mathbf{c}$ ($\mathbf{E}_1 \perp \mathbf{c}$) toward $\mathbf{B}_0 \perp \mathbf{c}$ ($\mathbf{E}_1 \perp \mathbf{c}$) the line broadens due to a decrease in the effective g factor and the microwave power transmitted through the sample decreased owing to the increase in the absorption associated with water in the channels. The combination of these factors led to a limited range of angles in the measurement of the angular dependence of the spectra. To eliminate the effect of absorption by water, we subjected the sample to dehydration. After annealing, the crystal acquired a milk-white color

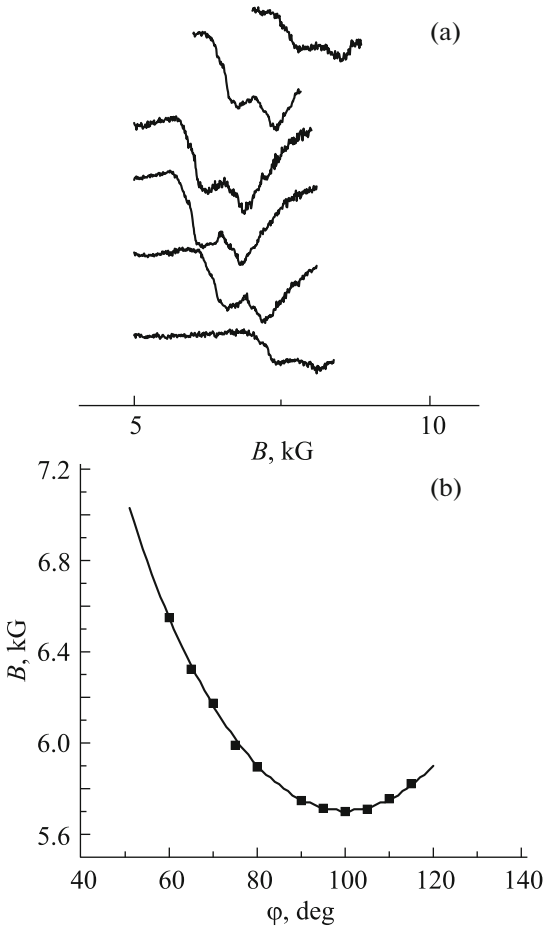

Fig. 3. (a) The ESR spectra of Fe^{2+} ions in a beryl crystal (sample 2, rotation in the *ac* plane with a step of 20°). The spectra in the lowest magnetic field correspond to the orientation close to $\mathbf{B}_0 \| \mathbf{c}$. (b) The angular dependence of the singlet–doublet resonance transition of Fe^{2+} ions in beryl (sample 4). The frequency is 395.5 GHz.

owing to a large number of microcracks and broadband absorption in the region of the ESR spectra in the polarization $\mathbf{E}_1 \perp \mathbf{c}$ disappeared. However, at the same time, the ESR spectra transformed. First, the ESR lines narrowed and their structure disappeared and, second, the ESR signal intensity decreased, which prevented extending the range of angles for the orientation dependence. Figure 1 shows the ESR spectra before and after dehydration for comparison.

3.2. Optical Spectroscopy

Figure 4 shows the absorption spectra of three different beryl samples. As far as their configuration and position of absorption lines are concerned, they are identical to the spectra described in a number of earlier works on the investigation of the optical properties of undoped and iron or vanadium-doped beryls [21–23].

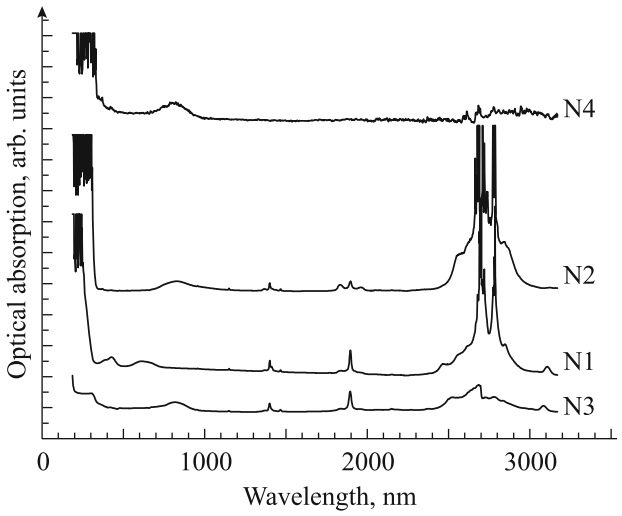

Fig. 4. Optical absorption spectra of various beryl samples.

As is seen in Fig. 4, all presented spectra exhibit absorption in the ultraviolet (UV) range of wavelengths of 250–350 nm, which is caused by the ligand-to-metal charge transfer in the FeO_n polyhenda (where $n = 6$ or 4). Despite some debate in the literature concerning interpretation of these or those absorption bands in the UV range, all researchers agree that the short-wavelength absorption in the spectra of beryls is largely determined by the $O^{2-} \rightarrow Fe^{3+}_{VI}$ charge transfer. A lesser contribution to the UV absorption comes from the charge transfer bands $O^{2-} \rightarrow Fe^{3+}_{IV}$, Fe^{2+}_{IV} (at the isomorphic inclusion of trivalent and bivalent iron ions in the beryllium tetrahedra of the structure). Thus, the presence of a more intense shortwave absorption in the optical spectra of synthetic samples 1 and 2 compared to the natural sample implies that a major fraction of the iron impurity in these samples occurs in the trivalent state and isomorphically substitutes aluminum or beryllium cations.

The optical response of non-Kramers Fe^{2+} ions is of particular interest. It is commonly accepted that bivalent iron ions are manifested in the beryl spectrum by a wide band in the near infrared wavelength range with an absorption peak at 820 nm. The emergence of this band is associated with the electronic transitions $^5T_2 \rightarrow {}^5E$ in the energy spectrum of the Fe^{2+}_{VI} ion isomorphically substituting aluminum in the octahedral positions of the structure [22]. It is worth mentioning that this absorption band, whose edge extends to the long-wavelength "red" region of the visible range, causes blue tints in the color gamma of beryl. As follows from Fig. 4, this band appears in the spectra of both bluish synthetic sample 2 and natural beryl, which indicates the presence of bivalent iron ions in these samples. This band is completely absent in the

spectrum of green sample 1. The optical spectrum of this sample is, in contrast, characterized by the presence of two other pronounced absorption bands. The first of them, the shortwave one, is situated at about 420–425 nm, whereas the intensity maximum of the second absorption band falls to the wavelength interval of 560–580 nm. According to the literature data [23], the presence of absorption bands at 425 and 580 nm in the optical spectrum of green beryl indicates the presence of trivalent vanadium ions in this sample, which occupy the octahedral positions of aluminum in the crystal structure; namely, the band in question are explained by the electronic transitions of $^3T_{1g}(^3F) \rightarrow {}^3T_{1g}(^3P)$ and $^3T_{1g}(^3F) \rightarrow {}^3T_{2g}(^3F)$, respectively, in V^{3+}_{VI} ions [23].

In addition to the absorption bands described above, the spectral dependences shown in the figure feature three more absorption bands lying in the near infrared wavelength range and typical for natural beryl crystals and the crystals grown by the hydrothermal method. The two first of them seen as narrow structured absorption bands at 1400 and 1898 nm, respectively, are caused by higher overtones in the vibrational spectrum water molecules embedded in the structural channels of beryl [24]. The additional absorption bands situated at wavelength of 1836 and 1960 nm belong to absorption by type I water (the electric dipole moments of type I and type II water molecules are situated perpendicular and parallel to sixth order axis, respectively) in the structural channels of beryl. The third (most intense and broad) absorption band in the wavelength range from 2500 to 3000 nm is induced by structureless oscillations of water situated in various gas-liquid inclusions in beryl. High-temperature annealing results in dehydration of the beryl crystal and its partial destruction at a microscopic level. The absorption lines due to the structural water in the channel in annealed sample 4 completely disappear, whereas the broad IR abruption line due to the gas inclusions is red-shifted owing to their growth and microscopic destructions up to a maximum wavelength of 3200 nm achievable in our optical measurements. In this case, a large number of microcracks lead to a considerable increase in the optical density of the crystal in the entire wavelength range under investigation. It is important to mention here that the absorption band at 820 nm due to bivalent iron ions, which is most interesting for our ESR measurements, also considerably broaden as a result of annealing. Broadening of the absorption band at 820 nm implies that distortion of the octahedral position of beryl and its entire structure occurred under heating of the sample owing to thermal expansion under the thermal impact.

4. DISCUSSION

According to the data of the chemical analysis (see the table), there was an iron impurity in both synthetic beryl samples (samples 1 and 2); therefore, the reason of the absence of the signal in sample 1 should be understood. In our opinion, it is associated with a lower (by a factor of 7) impurity density. In addition, sample 1 was grown at a higher oxidation potential and, as a result, the fraction of Fe^{3+} in this sample can be much higher than in sample 2, which further decreases the fraction of Fe^{2+}. Taking into account a fairly low signal-to-noise ratio for sample 2, the absence of the ESR signal in sample 1 is quite reasonable. On the other hand, the ESR signal observed in goshenite indicates that, if the impurity occurs predominantly in the bivalent state, its detection is possible even at a low iron density.

Since the ESR spectra of trivalent iron and Fe^{3+}–Fe^{3+} exchange pairs are known and cannot explain the signals observed in the submillimeter range, it can be concluded that the observed spectra belong to isolated Fe^{2+} ions (the electronic configuration d^6, the main term ^5D). To determine the type of the crystallographic position, in which the bivalent iron ions occur, we take into account the presence of splitting between the levels of the doublet. This manifests a rhombic component of the local symmetry; i.e., the octahedral coordination with the symmetry D_3 can be excluded with a high probability. The tetrahedral positions permit the splitting of the doublet, but the substitution $Si^{4+} \rightarrow Fe^{2+}$ requires a charge compensation for the silicon-oxygen tetrahedral, which should lead to the emergence of conjugate spectra with the magnetic axes directed at oblique angles to the compensators. In the case of beryllium tetrahedron, magnetically nonequivalent centers should also exist, but the magnetic axes of the centers should be directed along $\langle 2\bar{1}\bar{1}0\rangle$, $\langle 10\bar{1}0\rangle$, and [0001] for isovalent substitution. In this case, since the ESR spectra cannot be detected in the experiment at the direction of the magnetic field perpendicular to the C axis of the crystal, the observed isolated spectrum can be explained under the condition that the Z axes of the observed centers are directed along the sixth-order axis. Further discussion is based on the assumption that the Fe^{2+} ion substitutes beryllium in the tetrahedron. If it is the case, the ground orbital state in the cubic field is the doublet Γ_3. Under the action of the low-symmetry components of the crystal field, the doublet splits and the five-fold spin-degenerate singlet should become the ground orbital state. The spin–orbital interaction lifts the spin degeneracy in the second order and leads to a system of spin sublevels characterized by spin $S = 2$ [25]. This approach allows describing, e.g., the experimental results on the far infrared spectroscopy of the $Fe(SPh)_4^{2-}$ compound [26]. On the other hand, position of low-lying energy levels of Fe^{2+} centers in undistorted tetrahedra with the symmetry T_d (ZnS, CdTe, $MgAl_2O_4$), where the main contribution to the splitting of the orbital doublet comes from the second-order spin–orbit interac-

tion, was previously studied experimentally and theoretically [4, 27]. Five equidistant energy levels with the symmetry Γ_1, Γ_4, Γ_3, Γ_5, and Γ_2 were discovered in these compounds and the ground-state singlet Γ_1 was separated from the excited-state triplet Γ_4 by energy interval of ($ZnS : Fe^{2+}$) 15, (CdTe) 10, and ($MgAl_2O_4$) 13 cm^{-1}. Recent measurements of the ESR spectra in $ZnSe : Fe^{2+}$ allowed us to supplement this set and measure the splitting between the singlet and triplet, which turned out to be approximately 15.5 cm^{-1} [28]. Comparing these values with the zero-field splitting in beryl (12.7 cm^{-1}) one can notice the closeness of the measured values. In addition, an extra weak broad line detected in this work with the zero-field splitting greater than the one of the doublet can be associated with splitting of the triplet into a doublet and a singlet in the rhombic field. It is worth mentioning that the splitting between the levels of the doublet in our case is small and the presence of the singlet–singlet transition with the zero-field splitting close to the respective value of the singlet–doublet transition cannot be described by the level scheme with the spin $S = 2$. It can be suggested that the level system of Fe^{2+} in beryl is nearly the same as in cubic crystals and the action of the low-symmetry components of the crystal field is a perturbation. Such a level scheme takes place, e.g., in hexagonal $GaN : Fe^{2+}$ [29], where the excited triplet Γ_4 is split by the trigonal field into the doublet Γ_3 and the singlet Γ_2.

Since the position of the singlet–singlet lines was determined with a large error and the number of measured points was insufficient for calculations, we used for the theoretical only the resonance transitions of the singlet–doublet type. The calculation was carried out in the approximation of the effective spin $S = 1$. The spin Hamiltonian had of the form

$$H = g_{\|}\beta B_z S_z + g_{\perp}\beta(B_x S_x + B_y S_y) + D[S_z^2 - S(S+1)/3] + E(S_x^2 - S_y^2).$$

The parameters of the Hamiltonian were found in two stages. First, we found $g_{\|} = g_c = 2.0 \pm 0.1$, $D = 379.5$ GHz and $E = 1.3$ GHz from the experimental frequency–field dependence (Fig. 2). To determine the transverse g factor we used the angular dependence measured at a frequency of 355.5 GHz and found $g_{\perp} = 3.7 \pm 0.5$. The respective curves calculated with the use of MATLAB software are shown by solid lines in Figs. 2 and 3. Despite fair agreement, it is necessary to mention that the accuracy of finding $g_{\perp}$ is low owing to the fact that the Zeeman energy makes only a small contribution to the energy of the resonance transition and the frequency error (±0.5 GHz) is quite large in this case. This question is considered in detail in [30]. Observation of the ESR line belonging to the Fe^{2+} ions in iron-containing samples grown by the flux method with a lack of BeO in the initial charge was reported earlier in [9]. It is worth mentioning first of all that the very observation of the ESR spectra of Fe^{2+} at room temperature is unusual. In [9], a line with $g_c = 3.773$ was detected and attributed to the resonance transition $-1 \rightarrow +1$ of Fe^{2+} ions in the position of Be^{2+} in the model describing the spin sublevels by the total spin $S = 2$. Although they also failed to measure the complete angular dependence, they discoverd the magnetic multiplicity ($K_M = 3$) of the spectra, whereas we did not observed magnetically nonequivalent centers. Thus, it can be concluded that we deal with another center in this case. Since our interpretation contradicts with the results of [9], the question of identification of the spectra of Fe^{2+} can be definitely solved after the observation of other excited levels.

It is necessary to mention that, although the recalculated formula of sample 2 does not include iron in the beryllium position, the accuracy of the chemical analysis is insufficient to exclude it completely. Taking into account that the ESR signals are very weak, this contradiction can be disregarded.

The nature of the ESR line structure has not been established. In the measurement of the frequency–field dependence of the ESR spectra, it turned out that the distance between the components does not change and each component should possess its own zero-field splitting. This implies that there are several crystallographic positions in the crystal occupied by bivalent iron ions with tiny changes in the nearest neighborhood. Since the line structure disappeared after dehydration of the crystal, it can be concluded that water molecules affect the crystal field of the ligands surrounding Fe^{2+} ions; i.e., the water molecules in channels either slightly deform the crystal matrix or, owing to their large dipole moment, introduce a distortion to the crystal field potential acting on the Fe^{2+} ion. It is worth mentioning that investigations of impurity ions in beryl by ESR are carried out for a long time and such an influence of water was not reported so far. However, large zero-field splittings were not measured in those works and the effects induced by the presence of slightly different centers in the case of the use of standard ESR spectrometers can be within the line width. Although natural goshenite exhibits specific lines of water in the channels (Fig. 4), the signal-to-noise ratio of the ESR spectra of Fe^{2+} is too low to analyze the line shape.

5. CONCLUSIONS

Fe^{2+} centers with a rhombic symmetry have been identified in a synthetic $Be_3Al_2Si_6O_{18} : Fe$ crystal and natural goshenite. It has been concluded that bivalent iron ions isovalently substitutes beryllium in the position of the oxygen tetrahedron. The set of spectrum parameters has been determined, which provide agreement of the theory and the experiment. A separate investigation is required to establish the nature of a change in the ESR line shape after dehydration.

ACKNOWLEDGEMENTS

This work was supported by the Russian Foundation for Basic Research (project no. 14-02-00255) and the Ministry of Education and Science of the Russian Federation (the "5top100" program and the State order no. 3.9896.2017/VU).

REFERENCES

1. R. Doerfler, G. R. Allan, B. W. Davis, C. R. Pidgeon, and A. Vass, J. Phys. C **19**, 3005 (1986).
2. G. S. Shakurov, T. A. Shcherbakova, and V. A. Shustov, Appl. Magn. Reson. **40**, 135 (2011).
3. B. R. Anderson and L. J. Challis, J. Phys. C **6**, L266 (1973).
4. G. A. Slack, S. Roberts, and F. S. Ham, Phys. Rev. **155**, 170 (1967).
5. W. Low and M. Weger, Phys. Rev. **118**, 1130 (1960).
6. M. M. Zaripov and Yu. Ya. Shamonin, Izv. Akad. Nauk SSSR, Ser. Fiz. **20**, 1220 (1956).
7. M. Dvir and W. Low, Phys. Rev. **119**, 1587 (1960).
8. A. Edgar and D. R. Hutton, Solid State Commun. **41**, 195 (1982).
9. V. P. Solntsev, G. V. Bukin, G. G. Lokhova, and N. S. Veis, Tr. IGiGSO RAN, No. **610**, 128 (1985).
10. B. P. Gorshunov, E. S. Zhukova, V. I. Torgashev, V. V. Lebedev, G. S. Shakurov, R. K. Kremer, E. V. Pestrjakov, V. G. Thomas, D. A. Fursenko, and M. Dressel, J. Phys. Chem. Lett. **4**, 2015 (2013).
11. E. S. Zhukova, B. P. Gorshunov, V. I. Torgashev, V. V. Lebedev, G. S. Shakurov, R. K. Kremer, E. V. Pestrjakov, V. G. Thomas, D. A. Fursenko, and M. Dressel, J. Chem. Phys. **140**, 224317 (2014).
12. B. P. Gorshunov, V. I. Torgashev, E. S. Zhukova, V. G. Thomas, M. A. Belyanchikov, C. Kadlec, F. Kadlec, M. Savinov, T. Ostapchuk, J. Petzelt, J. Prokleska, P. V. Tomas, E. V. Pestrjakov, D. A. Fursenko, G. S. Shakurov, A. S. Prokhorov, V. S. Gorelik, L. S. Kadyrov, V. V. Uskov, R. K. Kremer, and M. Dressel, Nat. Commun. **7**, 12842 (2016).
13. R. I. Mashkovtsev, E. S. Stoyanov, and V. G. Tomas, Zh. Strukt. Khim. **45**, 59 (2004).
14. R. I. Mashkovtsev, L. V. Kulik, and V. P. Solntsev, J. Struct. Chem. **51**, 869 (2010).
15. K.-T. Vil'ke, *Methods of Growing Crystals* (Nedra, Leningrad, 1977) [in Russian].
16. V. A. Klyakhin, A. S. Lebedev, A. G. Il'in, and D. A. Fursenko, USSR Inventor's Certificate No. 126565 (1979).
17. V. G. Tomas and V. A. Klyakhin, in *Mineral Formation in Endogenous Processes, Collection of Articles,* Ed. by N. V. Sobolev (Nauka, Novosibirsk, 1987), p. 60 [in Russian].
18. O. N. Lopatin, R. I. Khaibullin, F. G. Vagizov, V. V. Bazarov, A. I. Bakhtin, and I. B. Khaibullin, Zapiski VMO **4**, 122 (2001) [in Russian].
19. R. I. Khaibullin, O. N. Lopatin, F. G. Vagizov, V. V. Bazarov, A. I. Bakhtin, I. B. Khaibullin, and B. Aktas, Nucl. Instrum. Methods Phys. Res. B **206**, 277 (2003).
20. V. F. Tarasov and G. S. Shakurov, Appl. Magn. Reson. **2**, 571 (1991).
21. A. N. Platonov, M. N. Taran, and V. S. Balitskii, *The Nature of the Coloration of Gems* (Nedra, Moscow, 1984) [in Russian].
22. A. N. Platonov, M. N. Taran, E. V. Pol'shin, and O. E. Min'ko, Izv. Akad. Nauk SSSR, Ser. Geol. **10**, 54 (1979).
23. A. H. Platonov and A. N. Tarashchan, Konstit. Svoistva Miner. **7**, 75 (1973).
24. D. L. Wood and K. Nassau, Am. Mineral. **53**, 777 (1968).
25. A. Abragam and B. Bleaney, *Electron Paramagnetic Resonance of Transition Ions* (Oxford Univ. Press, London, 1970), Vol. 1.
26. P. M. Champion and A. J. Sievers, J. Chem. Phys. **66**, 1819 (1977).
27. G. A. Slack, F. S. Ham, and R. M. Chrenko, Phys. Rev. **152**, 376 (1966).
28. G. S. Shakurov, D. S. Pytalev, V. I. Kozlovsky, and Yu. V. Korostelin, in *Modern Development of Magnetic Resonance, Proceedings of the International Conference, Kazan, Russia, 2015,* p. 131.
29. E. Malguth, A. Hoffmann, and X. Xu, Phys. Rev. B **74**, 165201 (2006).
30. G. S. Shakurov, A. G. Avanesov, and S. A. Avanesov, Phys. Solid State **51**, 2292 (2009).

Translated by A. Safonov